JOURNAL OF GEOPHYSICAL RESEARCH, VOL. 103, NO. C2, PAGES 3203–3215, FEBRUARY 15, 1998

Observations of sand bar evolution on a natural beach

Edith L. Gallagher

Oceanography Department, Naval Postgraduate School, Monterey, California

Steve Elgar

School of Electrical Engineering and Computer Science, Washington State University, Pullman

R.T. Guza

Center for Coastal Studies, Scripps Institution of Oceanography, La Jolla, California

Abstract. Waves, currents, and the location of the seafloor were measured on a barred beach for about 2 months at nine locations along a cross-shore transect extending 255 m from 1 to 4 m water depth. The seafloor location was measured nearly continuously, even in the surf zone during storms, with sonar altimeters mounted on fixed frames. The crest of a sand bar initially located about 60 m from the shoreline moved 130 m offshore (primarily when the offshore significant wave height exceeded about 2 m), with 1.5 m of erosion near the initial location and 1 m of accretion at the final location. An energetics-type sediment transport model driven by locally measured near-bottom currents predicts the observed offshore bar migration, but not the slow onshore migration observed during low-energy wave conditions. The predicted offshore bar migration is driven primarily by cross-shore gradients in predicted suspended sediment transport associated with quasi-steady, near-bottom, offshore flows. These strong (> 50 cm/s) currents, intensified near the bar crest by wave breaking, are predicted to cause erosion on the shoreward slope of the bar and deposition on the seaward side. The feedback amoung morphology, waves, circulation, and sediment transport thus forces offshore bar migration during storms.

1. Introduction

Sand bars are an important morphologic feature of natural beaches. At many sites, changes in bar position and height are the primary source of beach profile variability [*Holman and Sallenger*, 1993]. Bars also effect significantly cross-shore wave transformation and the subsequent profile evolution [*Takeda and Sunamura*, 1987; *Seymour*, 1987]. However, the formation and evolution of sand bars are understood poorly. *Holman and Sallenger* [1993] review hypotheses for sand bar formation and conclude that both the break-point [*Dyhr-Nielsen and Sorenson*, 1970] and the infragravity wave [*Holman and Bowen*, 1982, and references therein] mechanisms may be important. The present work concerns the evolution of an existing sand bar.

Sand bars on natural beaches typically move slowly shoreward when wave energy is low and move more rapidly offshore when waves are energetic and the wave-driven circulation is strong [*Winant et al.*, 1975; *Aubrey*, 1979; *Jaffe et al.*, 1984; *Wright and Short*, 1984; *Lippmann and Holman*, 1990]. Although the net direction of bar motion is known from prestorm and poststorm bathymetric surveys, continuous observations of the bathymetric evolution of a natural beach during high-energy waves have only recently been obtained by using downward looking sonar altimeters mounted on fixed frames [*Gallagher et al.*, 1996]. Here, about 2 months of nearly continuous observations with nine altimeters (and colocated current meters) are used to describe and model bar-dominated bathymetric evolution on a cross-shore transect extending from about 1- to 4-m water depth.

Models for the evolution of the cross-shore profile (including sand bars) include equilibrium profile [*Bruun*, 1954; *Dean*, 1977], descriptive [*Wright and Short*, 1984; *Lippmann and Holman*, 1990], empirical beach profile evolution [*Kriebel and Dean*, 1985; *Kraus and Larson*, 1988], and process-based models [*Bowen*, 1980; *Bailard*, 1982; *Dally and Dean*, 1984; *Watanabe and Dibajnia*, 1988; *Roelvink and Stive*, 1989; *Thornton et al.*, 1996]. *Roelvink and Brøker* [1993] review profile evolution models. Process-based models attempt to account explicitly for the physical processes effecting bathymetric evolution. Process-based energetics-type sediment transport models (based on *Bagnold* [1966], described in section 3 below) relate sediment transport

Paper number 97JC02765.
0148-0227/98/97JC-02765$09.00

to the near-bottom flow field and have been used often to predict morphological evolution. *Bowen* [1980] demonstrated that the cross-shore variation of beach slope and sediment size are better predicted by an energetics model than by a null-point model [*Eagleson and Dean*, 1961]. Improved predictions of profile changes using the energetics transport model are reported to result from including (in the wave and wave-driven circulation models) undertow [*Stive and Battjes*, 1984], wave asymmetry [*Stive*, 1986; *Nairn and Southgate*, 1993], breaking-induced turbulence [*Roelvink and Stive*, 1989], and infragravity waves [*Sato and Mitsunobu*, 1991]. *Roelvink and Stive* [1989] compared cross-shore profile evolution observed in the laboratory with predictions of an energetics-type model. The near-bottom flows (predicted with a different model) driving the sediment transport included all of the above processes. *Roelvink and Stive* [1989] concluded that the vertically integrated, instantaneous response of the modeled sediment transport to the near-bottom flow assumed in the energetics transport model was of limited validity in the nearshore. However, performance of the sediment transport model is difficult to evaluate in studies where the predicted transport also depends on the accuracy of the hydrodynamic models.

Sediment suspension observed in the surf zone is spatially and temporally intermittent. Large changes in concentration occur over times shorter than a wave period [e.g., *Downing et al.*, 1981] and at spatial scales shorter than a wavelength, even in the absence of well-formed orbital ripples [*Conley and Inman*, 1992; *Hay and Bowen*, 1995]. The causes of these fluctuations in suspended sediment concentration are unclear and may include instabilitites of the bottom boundary layer [*Conley and Inman*, 1994; *Foster et al.*, 1995], vortex shedding from megaripples, or coherent turbulent flow structures [*Hay and Bowen*, 1994]. The sediment transport model [*Bagnold*, 1966] underlying exisiting process-based profile evolution models does not predict accurately the time history of sediment transport on a wave-by-wave basis. However, the time-averaged versions of these transports that are used in profile evolution models can still be useful [e.g., *Bowen*, 1980; *Thornton et al.*, 1996].

Dally and Dean [1984], *Sallenger and Howd* [1989], and others have suggested that bar formation and migration is caused by offshore directed, near-bottom, breaking wave-driven steady flows ("undertow"). However, undertow is not understood well even on planar beaches where the wave transformation is parameterized well [e.g., *Stive and Wind*, 1986; *Svendsen and Buhr Hansen*, 1988; *Masselink and Black*, 1995]. On barred beaches, wave-breaking is enhanced near the bar crest and reduced in the bar trough [*Lippmann et al.*, 1996], and bar-intensified undertow has been observed [*Sallenger and Howd*, 1989; *Smith et al.*, 1992; *Haines and Sallenger*, 1994]. *Thornton et al.* [1996] used near-bottom velocities observed for 10 days on a densely instrumented cross-shore transect on a barred beach near Duck, North Carolina, to drive an energetics transport model. The morphology was usually measured daily with the CRAB (a large amphibious vehicle), but there were up to 48 hours between some surveys because the CRAB cannot operate when the significant wave height H_s exceeds about 2 m [*Lee and Birkemeier*,1993]. The modeled distribution of offshore directed transport was similar to the cross-shore distribution of the undertow, which was strongest near the bar crest. The model predicted the offshore migration of the sand bar observed during high-energy waves and strong mean flows, but not the onshore bar motion and other small profile changes observed during low-energy conditions.

The present study supports and extends the results of *Thornton et al.* [1996]. Currents observed on the same Duck beach (the observations are described in section 2) are used to drive the same energetics sediment transport model (described in section 3). Cross-shore varying sediment grain fall velocity is included in the present model and improves predictions of beach profile change. The nearly continuous observations of the currents and cross-shore profile allow comparison of measured and predicted beach profiles during storms, as well as between them. Observed and modeled beach profile changes are compared (section 4) for four several-day-long events, and for a continuous 60-day period. Offshore bar migration during storms and strong currents is predicted well. Cross-shore gradients in the modeled suspended sediment transport terms, caused by bar-intensified undertow, are the dominant terms contributing to offshore bar migration. Onshore bar migration during calm periods is predicted poorly. Megaripples (observed with a small array of seven altimeters in the trough shoreward of the sand bar, see section 2) were present during low and high wave conditions. The effects of bedforms and fluid accelerations on sediment suspension could contribute to poor model performance when oscillatory currents are larger than steady currents. The results are summarized in section 5.

2. Observations

The data were obtained during the Duck94 field experiment conducted near Duck, North Carolina on a barrier island exposed to the Atlantic Ocean. Colocated sonar altimeters, pressure sensors, and bidirectional Marsh-McBirney electromagnetic current meters, sampled at 2 Hz, were deployed on fixed frames at nine locations on a 255-m-long cross-shore transect. Colocated pressure and current meters (but no altimeter) were deployed at four additional locations along the transect (Figure 1). The average spacing between flowmeters (about 25 m) was approximately 20% less than in the work of *Thornton et al.* [1996]. Current meters were raised and lowered as the bed level changed, maintaining an elevation above the seafloor between 40 and 100 cm. The seafloor location directly under each altimeter (averaged over the approximately 6-cm-diameter circular footprint) was estimated from the altimeter data using algorithms described by *Gallagher et al.* [1996]. Temporal averaging of the seafloor location estimates ranges from 32 s to 24 hours. The altimeter-based

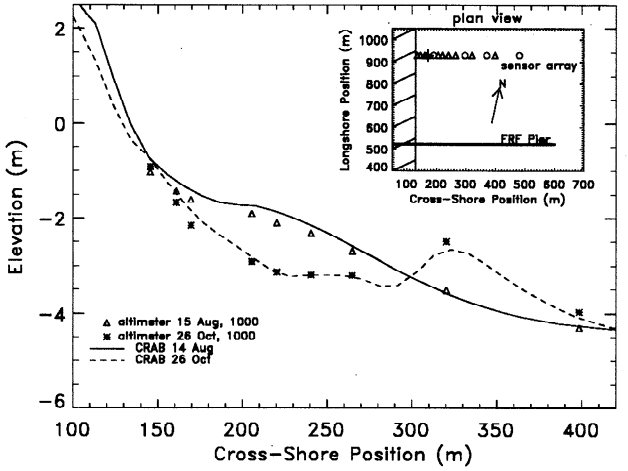

Figure 1. Elevation of the seafloor (relative to mean sea level) versus cross-shore position. The solid (Aug 14) and dashed (Oct 26) curves are CRAB profiles and triangles (Aug 15) and asterisks (Oct 26) are 3-hour average altimeter profiles. The inset shows a plan view of instrument locations. Colocated pressure sensors, current meters, and altimeters are indicated with triangles, colocated pressure and current meters with circles, and a small two-dimensional array of altimeters with a plus.

cross-shore profiles are spatially sparse, but still resolve features observed in spatially dense (but less frequent) CRAB profiles (Figure 1).

Between August 15 and October 26 the bar crest moved 130 m offshore with 1.5 m of erosion near the initial location and 1 m of accretion at the final location (Figure 1). Offshore migration (Figures 2a and 2b) occurred primarily during high-energy wave conditions ($H_s > 2$ m, Figure 2d). Slight onshore bar movement occurred with low-energy waves. Offshore bar migration rates, based on the location of the bar crest estimated from successive 3-hour profiles, were larger than the onshore migration rates (Figure 2b). The estimates of bar crest position and migration speed (especially the low speeds associated with slight onshore bar motion) are only qualitative owing to the relatively large spatial separation between altimeters. CRAB profiles (when available) were used to improve the estimated bar crest locations.

With Δ_n the measured change in seafloor elevation at each of the N sensors along the cross-shore transect, the cross-shore mean (e.g., net) and root-mean-square (RMS) changes are

$$\Delta_{\text{net}} = \frac{1}{N}\sum_{n=1}^{N} S_n \Delta_n \qquad (1a)$$

$$\Delta_{\text{RMS}} = \sqrt{\frac{1}{N}\sum_{n=1}^{N} (S_n \Delta_n)^2} \qquad (1b)$$

The observed changes are weighted by

$$S_n = \frac{\frac{1}{2}(dx_{n-1} + dx_n)}{\bar{dx}}$$

where $dx_n = x_{n+1} - x_n$ is the separation between adjacent sensors and $\bar{dx}$ is the average sensor separation. If sand is conserved (e.g., no longshore transport divergence and no transport from within the array to locations shoreward or seaward of the array) and the profile is spatially sampled adequately, then $\Delta_{\text{net}} = 0$. Time series of Δ_{net} and Δ_{RMS} based on successive 24-hour average profiles show that daily Δ_{net} is usually less than half the daily Δ_{RMS} (Figure 2c). The mean and RMS changes (equation (1)) were also calculated by using profile changes Δ_n based on 3-hour average profiles from the beginning and end of events (Table 1). For the several-day bar motion events studied in detail

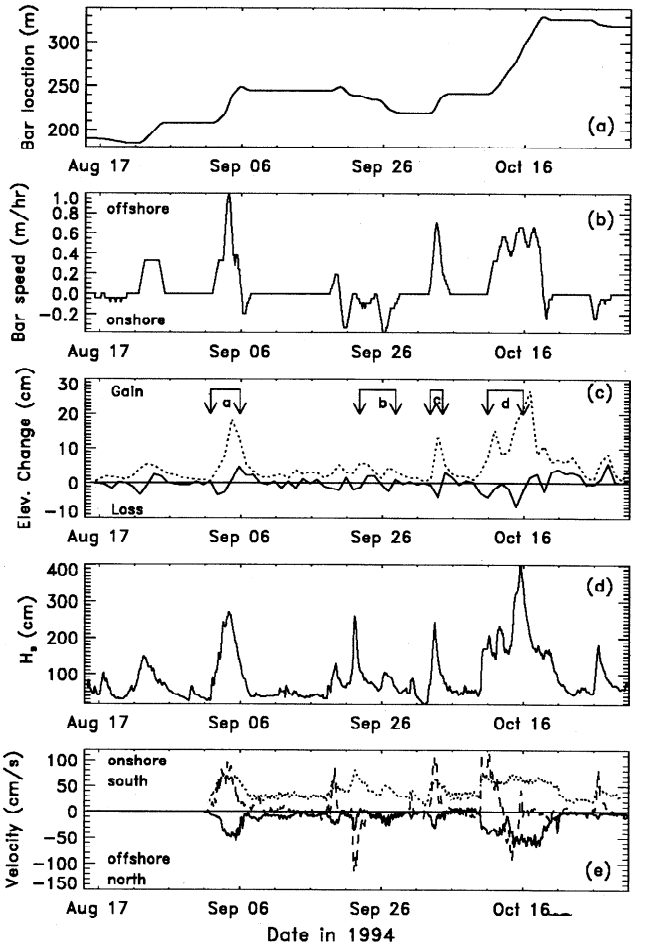

Figure 2. (a) Cross-shore location and (b) speed of migration of the sand bar crest (estimated from 3-hour average altimeter profiles) versus time. (c) Net (solid curve) and RMS (dashed curve) differences (equation (1)) between 24-hour average altimeter profiles. The periods labeled a, b, c, and d are discussed in the text. (d) Significant wave height (3-hour average) measured in 8-m water depth and (e) currents (3-hour average) measured near the bar crest. The dotted curve is the square root of the total velocity variance, the dashed curve is the mean longshore current (positive is southward flow), and the solid curve is the mean cross-shore current (positive is onshore flow). Currents were not measured before Sep 1, partially owing to a lightning strike that required retrieval, repair, and redeployment of many flowmeters.

Table 1. Net and RMS Beach Change, Model Skill, and Correlation

	Sept 1–5 a	Sept 9–22	Sept 22–27 b	Sept 28–Oct 2	Oct 2–4 c	Oct 5–10	Oct 10–15 d	Oct 16–20	Oct 21–25	Oct 26–28	Sept 1 – Oct 28
					Beach Change						
Δ_{net}	1.6	-7.9	4.6	0.2	-3.9	-5.1	-13.7	9.1	6.8	7.0	8.4
Δ_{RMS}	32.9	11.8	15.5	6.0	16.9	8.6	47.8	40.2	12.8	12.7	86.7
					Model Skill						
Constant W	0.30	-1.98	0.02	-0.27	0.23	-1.78	0.39	-0.19	-0.09	-0.20	...
Variable W	0.48	-0.75	0.02	-0.12	0.28	-0.70	0.66	0.30	-0.03	-0.02	0.44
					Correlation						
Constant W	0.78	...	0.13	...	0.74	...	0.95	...	...	...	...
Variable W	0.80	...	0.28	...	0.81	...	0.96	...	...	...	0.89

Δ_{net} (cm), Δ_{RMS} (cm) (based on 3-hour profiles at the beginning and end of the indicated time periods), and model skill (using constant or variable fall velocity W) for short periods (determined by amount of beach change and sensor availability) and for the entire 60-day period. The periods labelled a – d are discussed in detail and the correlation between modeled and observed profile changes (weighted by sensor separation) for those periods and for the entire 60-day period are also given.

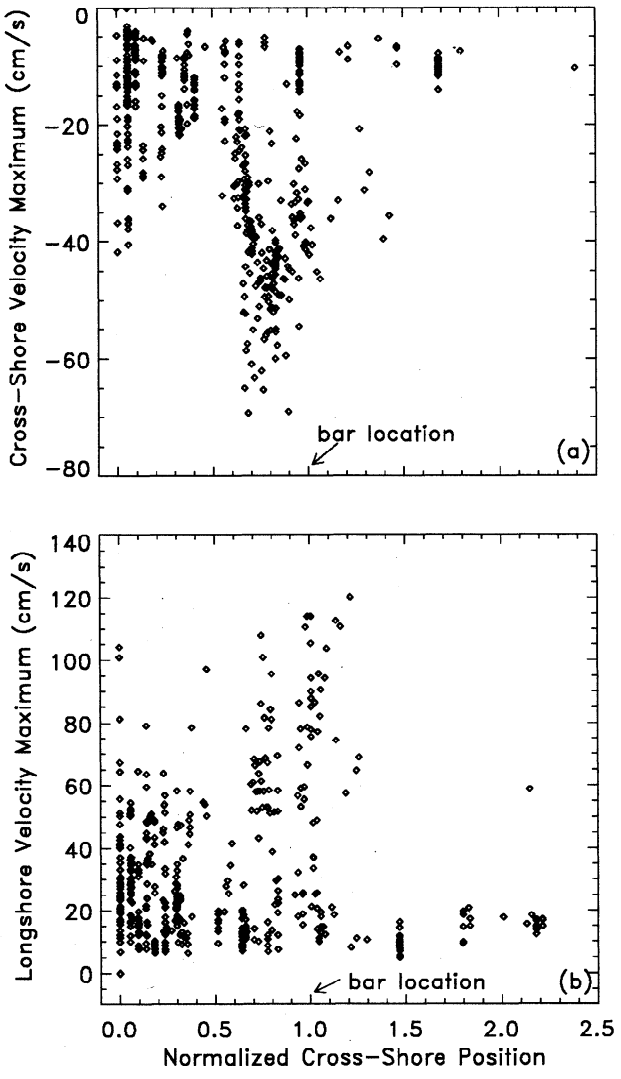

(a – d in Figure 2c, Table 1) and for the 2-month-long modeled period (September 1 to October 28, Table 1) the observed Δ_{net} is at least a factor of 4 smaller than Δ_{RMS}. Thus changes observed with the altimeters can largely be accounted for by redistribution of sediment along the cross-shore transect.

The largest changes in successive daily profiles (e.g., peaks in the daily Δ_{RMS}, Figure 2c) and the most rapid changes in bar location (Figure 2b) occur during storms when the offshore significant wave height is large (Figure 2d) and mean and oscillatory currents near the bar crest are strong (Figure 2e). When the magnitude of the observed cross-shore mean current was greater than about 10 cm/s, the maximum cross-shore mean current occurred just shoreward of the bar crest (Figure 3a). Although the cross-shore location of the maximum mean longshore current was more broadly distributed, the maximum was often located close to the bar crest (Figure 3b). These strong mean currents contribute significantly to the offshore bar motion predicted by the sediment transport model.

The four cross-shore transport events investigated in detail include three examples of offshore bar motion during relatively high-energy conditions (labeled a, c, and d in Figure 2c) and one case (b in Figure 2c) of onshore bar motion. Event d (October 10 – 15, Figure 2) includes a portion of the period with the largest ob-

Figure 3. Maximum 3-hour average near-bottom velocity for each 3-hour period between Sep 1 and Oct 31 versus location of the maximum. Locations are normalized such that $x = 1$ at the bar crest and $x = 0$ at the shallowest sensor (approximately 10–20 m from the shoreline). (a) Maximum offshore directed velocity and (b) absolute value of the maximum longshore velocity.

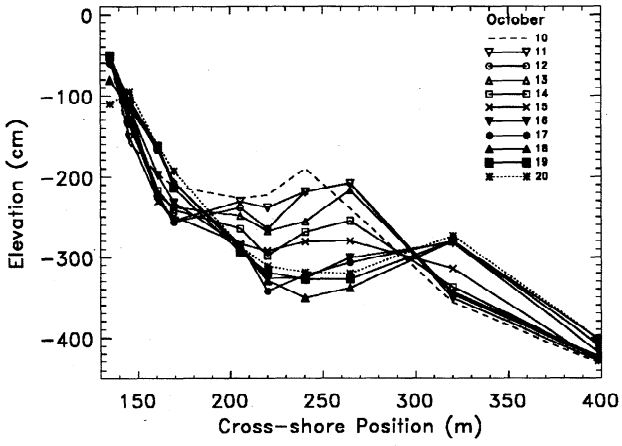

Figure 4. Elevation of the seafloor (relative to mean sea level) measured by sonar altimeters versus cross-shore position. One 3-hour average profile per day (2200–0100) is plotted for the 10-day storm period starting Oct 10 2200 (dates and line types are given in the legend).

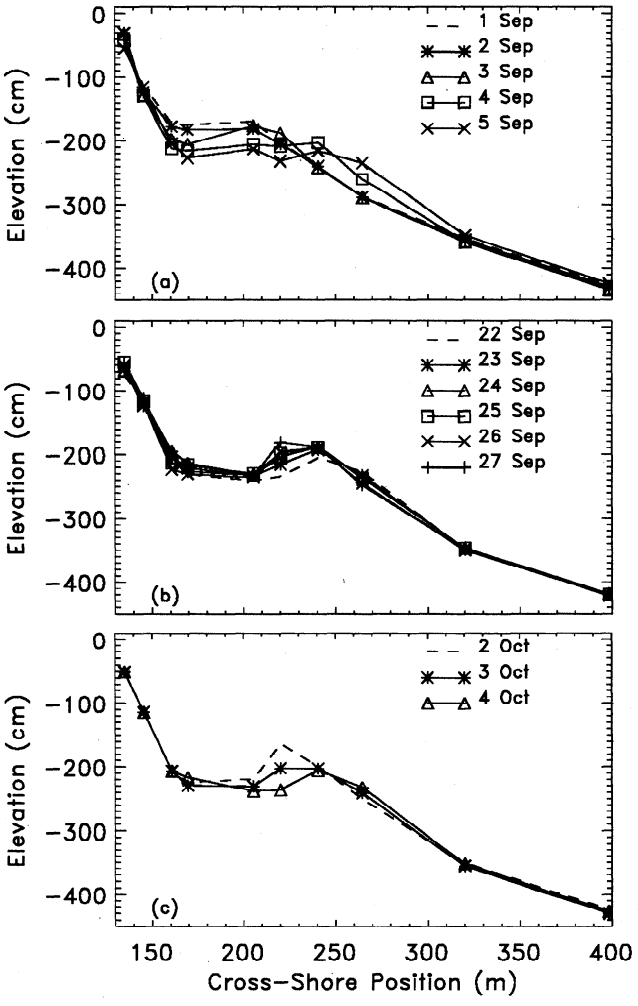

Figure 5. Elevation of the seafloor (relative to mean sea level) measured by sonar altimeters versus cross-shore position. One 3-hour average profile per day is plotted (dates and line types are given in legends). (a) Sep 1–5 (1900–2200), (b) Sep 22–27 (1900–2200), and (c) Oct 2–4 (1600–1900).

served profile change (October 10 – 20, Figure 4) and the largest observed H_s (4 m). During this storm, approximately 1.5 m of erosion occurred at the original location of the bar ($x = 240$ m, Figure 4) and 0.9 m of accretion occurred 80 m offshore at $x = 320$ m. The sand bar migrated steadily offshore and the profile evolved gradually (Figures 2b and 4), in contrast to suddenly or catastrophically as might occur if the sand bed were fluidized [*Seymour*, 1986]. The sand bar migrated offshore about 50 and 20 m during events a and c (Figures 5a and 5c, respectively), and migrated onshore about 20 m during event b (Figure 5b).

CRAB surveys on many cross-shore transects show the bathymetry was longshore homogeneous (i.e., the sand bar was approximately parallel to the shoreline) between August 25 and October 12, with little bathymetric change offshore of the most seaward altimeter. A CRAB survey on October 18 shows significant longshore bathymetric inhomogeneities developed during the storm.

Time series of seafloor location (e.g., Figure 6) measured with a two-dimensional 1.4 X 1.4 m coherent array of seven altimeters (located at $x = 170$ m, Figure 1) suggest migrating megaripples [*Hay and Wilson*, 1994] with heights of O(20 cm) were present during both high- and low-wave energy periods. Numerous visual observations confirmed the presence of megaripples with wavelengths of a few meters. The altimeter accuracy is about 2-3 cm

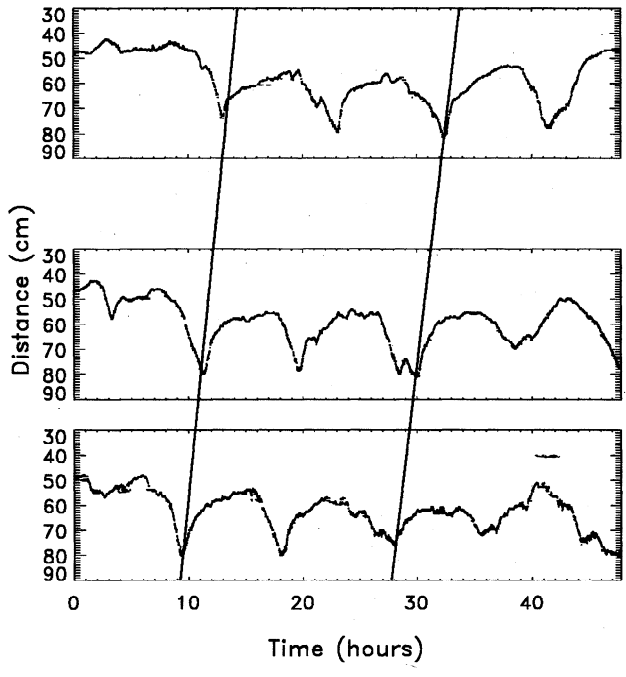

Figure 6. Distance to the seafloor (every 32 s between Sep 26 0100 and Sep 27 2200) below closely spaced altimeters in the 2-D array located at cross-shore location $x = 170$ m versus time. The altimeters are separated in the cross-shore direction by 80 (top to middle panel) and 60 cm (middle to bottom panel). Time series in the top panel are from the most onshore altimeter. Lines connecting the 'troughs' of the bedforms illustrate onshore migration of the features.

[*Gallagher et al.*, 1996]. However, 3-hour average estimates of the mean seafloor location (e.g., Figures 4 and 5) can contain errors of O(10 cm) owing to megaripples migrating slowly beneath the altimeters (shown in Figure 6). A longer averaging time would reduce errors by including more of the megaripple profile in the average, but would degrade the temporal resolution of the estimated profile changes. The megaripple observations, including migration rates and directions, will be discussed elsewhere.

3. Model

Assuming the energy dissipation of a unidirectional stream occurs via shear stress at the bed and that a fraction of the dissipated energy (or power) is used to move sediment, the total sediment transport rate i is [*Bagnold*, 1966]

$$i = i_b + i_s = \left(\frac{\epsilon_b}{\tan\phi - \tan\beta} + \frac{\epsilon_s(1-\epsilon_b)}{(W/\overline{u}) - \tan\beta} \right) \omega \quad (2)$$

where subscripts b and s refer to bedload and suspended load, β is the bed slope, ϕ is the angle of repose, and W is the sand grain fall velocity. The dissipated stream energy ω, equal to the product of the assumed quadratic shear stress at the bed ($\tau = \rho_w C_f |\overline{u}|\overline{u}$) and the mean free stream velocity $\overline{u}$, is

$$\omega = \tau\overline{u} = \rho_w C_f |\overline{u}|^3$$

where ρ_w is the water density and C_f is a friction coefficient. The efficiency factors ϵ_b and ϵ_s are the percent of power used for bedload and suspended load. Above a critical value of ω, *Bagnold* [1966] argued that $0.11 \leq \epsilon_b \leq 0.14$ and $\epsilon_s = 0.01$.

Bailard [1981] and *Bailard and Inman* [1981] extended the steady-flow transport equation (equation (2)) to combined (oscillatory and steady) flows. Assuming the beach slope is small, the resulting time-averaged, cross-shore volume sediment transport per unit width per unit time is [*Bailard*, 1981]

$$\begin{aligned} Q_x &= K_b \left\{ \langle |\vec{u}|^2 \tilde{u} \rangle + \langle |\vec{u}|^2 \overline{u} \rangle - \frac{\tan\beta}{\tan\phi} \langle |\vec{u}|^3 \rangle \right\} \\ &+ K_s \left\{ \langle |\vec{u}|^3 \tilde{u} \rangle + \langle |\vec{u}|^3 \overline{u} \rangle - \frac{\epsilon_s}{W} \tan\beta \langle |\vec{u}|^5 \rangle \right\} \quad (3) \end{aligned}$$

where $\vec{u}$ is the total (ie, cross-shore and longshore) near-bottom velocity vector, $\overline{u}$ and $\tilde{u}$ are the mean and oscillatory components of the cross-shore near-bottom velocity, respectively, $\tan\beta$ is the local cross-shore beach slope, and angle brackets indicate time average. The coefficients K_b and K_s are

$$K_b = \frac{\rho_w}{\rho_s - \rho_w} C_f \frac{\epsilon_b}{\tan\phi}; \qquad K_s = \frac{\rho_w}{\rho_s - \rho_w} C_f \frac{\epsilon_s}{W}$$

and ρ_s is the sand density.

Cross-shore sediment transport Q_x depends on longshore as well as cross-shore currents because both contribute to the total stress that mobilizes sediment. On the basis of comparisons of model predictions using offshore wave and current conditions with measured beach change, *Bailard* [1982] suggested that $\epsilon_b = 0.13$ and $\epsilon_s = 0.01$, similar to the results of *Bagnold* [1966], although the 95% confidence interval of these estimates was large. Following *Thornton et al.* [1996], here $\epsilon_b = 0.135$, $\epsilon_s = 0.015$, and $C_f = 0.003$ [*Church and Thornton*, 1993]. The present model predictions are not sensitive to ±30% changes in these parameters, nor to removing a few flowmeters, nor to plausible errors in the measured currents, as discussed in the Appendix.

Assuming there are no longshore gradients in longshore sediment flux and the density of sediment packing is constant, mass conservation in the cross-shore direction yields

$$\frac{dQ_x}{dx} = \mu \frac{dh}{dt} \quad (4)$$

where h is bed elevation and μ is a packing factor ($\mu = 0.7$ is used here [*Thornton et al.*, 1996]). As noted above, the bar was crescentic after October 18. However, little is known about the effects of alongshore variation in bathymetry on nearshore circulation and sediment transport, and further work (including additional data sets with more than one cross-shore transect) is needed to determine the importance of the neglected longshore sediment flux gradients. The assumption that cross-shore transport gradients are much larger than longshore transport gradients is supported by the fidelity of model predictions (discussed below) based on (4).

Thornton et al. [1996] predicted profile change at Duck (October 1990) with this model (equations (3) and (4)) initialized with CRAB profiles and driven by observed currents. Similarly, here the transport model is initialized with 3-hour average altimeter profiles and driven with observed currents. The model bed elevation change between adjacent current meters is calculated by using a finite difference scheme and then interpolated to approximate elevation change at the locations of the altimeters.

4. Model-Data Comparisons

The model performance is described by using both the correlation r between observed and predicted bed elevation change and the normalized RMS prediction error $E_{\mathrm{RMS}}/\Delta_{\mathrm{RMS}}$ (where E_{RMS} is the RMS error between predicted and observed final 3-hour averaged profiles, and Δ_{RMS} (1b) is the RMS change between the initial and final observed profiles). Specifically, a predictive skill is defined here as $1 - E_{\mathrm{RMS}}/\Delta_{\mathrm{RMS}}$ (similar to *Davis* [1976]). If the errors vanish, then skill = 1. The skill = 0 if the errors are as large as the observed changes, in which case the model prediction is not better than a prediction that the final profile equals the initial profile. The skill is negative if errors in the prediction

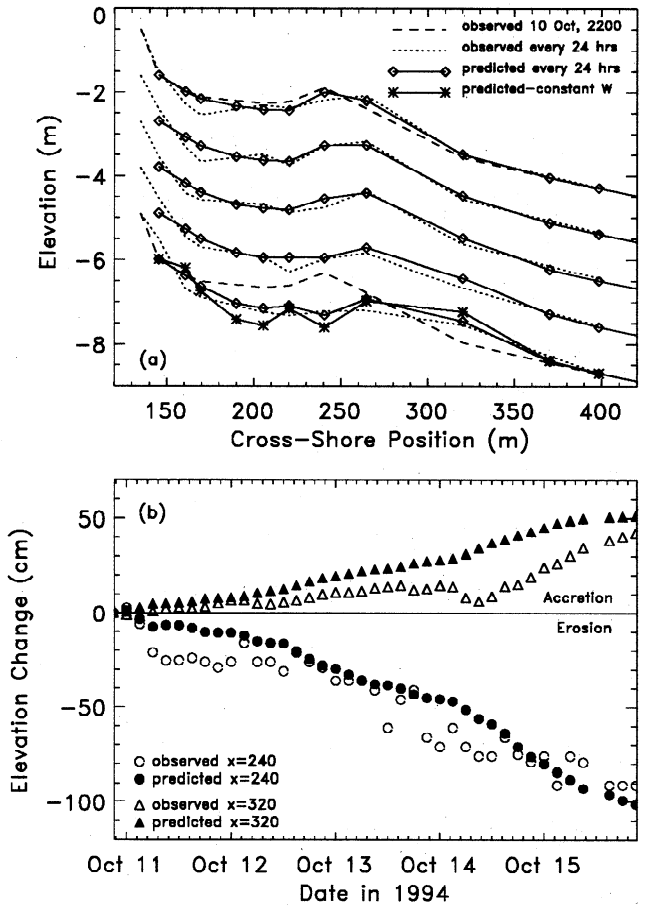

Figure 7. (a) Observed (dotted curves) and predicted (using varying W, solid curves with diamonds) elevation of the seafloor (relative to mean sea level) versus cross-shore position. Three-hour average profiles for each 24-hour period after model initialization (Oct 10 2200, dashed curve) are sequentially offset by -110 cm in the vertical. The final predicted profile using constant W (solid curve with asterisks) is also plotted. The initial profile (dashed curve) is superposed on the final profiles to show changes over the 5 days. (b) Observed (open symbols) and predicted (solid symbols) elevation at two cross-shore locations (circles, $x = 240$ m, location of maximum erosion and triangles, $x = 320$ m, location of maximum accretion) for every 3-hour period between Oct 10 2200 and Oct 15 2200 versus time.

are larger than the observed changes. The initial and final profiles that bracket periods of low wave energy can be similar (i.e., Δ_{RMS} is small), resulting in low skill (Table 1) even though the absolute errors in the predictions are not large. The statistics of predictive skill are unknown, and thus different values should be compared cautiously.

Using the same parameters as *Thornton et al.* [1996] (with the exception of fall velocities, discussed below), the model predicts accurately the overall profile changes and the offshore migration of the sand bar observed during a large storm (event d, October 10 – 15 1994, $H_s > 2$ m) (diamonds, Figure 7a). Although the conditions near the sand bar ($\overline{u}_{max} = 60$ cm/s, $\overline{v}_{max} = 100$ cm/s) were similar to those observed by *Thornton et al.* [1996] in 1990 ($\overline{u}_{max} = 50$ cm/s, $\overline{v}_{max} = 125$ cm/s), the model has much higher skill for the present data. *Thornton et al.* [1996] underpredict the observed erosion in the trough, whereas both erosion and accretion are predicted well here (Figure 7). *Thornton et al.* [1996] used the same value of the fall velocity ($W = 1.3$ cm/s) for all cross-shore locations except the shallowest, whereas here the cross-shore distribution of fall velocity was estimated (following *Sleath* [1984]) from sediment size measured along the transect (Table 2). The model skill for event d is 0.66 for spatially varying W (diamonds, Figure 7a), 0.39 for constant W (asterisks, Figure 7a), and approximately 0.14 for the constant W prediction shown for a 7-day event by *Thornton et al.* [1996, Figure 11]. For event d, a spatially varying W reduces RMS prediction errors by 50% relative to those with constant W. However, the corresponding correlations between observed and predicted elevation change are both high and not statistically different (Table 1). A spatially variable W results in higher skills and correlations for all predictions discussed here (Table 1, Figures 7a and 8), and results discussed below use variable W. Note that the correlations for predictions with variable W, although higher in every case, are not statistically different than the constant W predictions (Table 1).

In event a ($H_s = 2.8$ m and maximum offshore-directed currents ≈ 60 cm/s) the observed offshore migration of the sand bar from x=200 to x=250 m is predicted well, but erosion observed near the toe of the steep foreshore (x=170 m) is underpredicted (Figure 8a, skill=0.48, $r = 0.80$ (significant at the 95% level)). Time series of observed and predicted seafloor location (every 3 hours, Figure 9a) diverge as the bar moves past x=220 m (September 3–4 1200), but the final prediction is accurate. The small profile changes predicted for event c are considerably less than observed (Fig-

Table 2. Sediment Characteristics

Location, m	$\bar{d}$, mm	W, cm/s
135	0.29	3.9
145	0.26	3.5
160	0.25	3.3
170	0.25	3.3
190	0.25	3.3
205	0.22	2.8
220	0.22	2.8
240	0.18	2.0
265	0.18	2.0
300	0.18	2.0
320	0.17	1.6
370	0.16	1.5
400	0.16	1.5
480	0.15	1.3

Sediment characteristics as a function of cross-shore location from data collected in 1984–5 (Stauble 1991) and 1994 (Stauble, pers comm 1995). $\bar{d}$ is the mean grain size and W is the sediment fall velocity (after Sleath 1984).

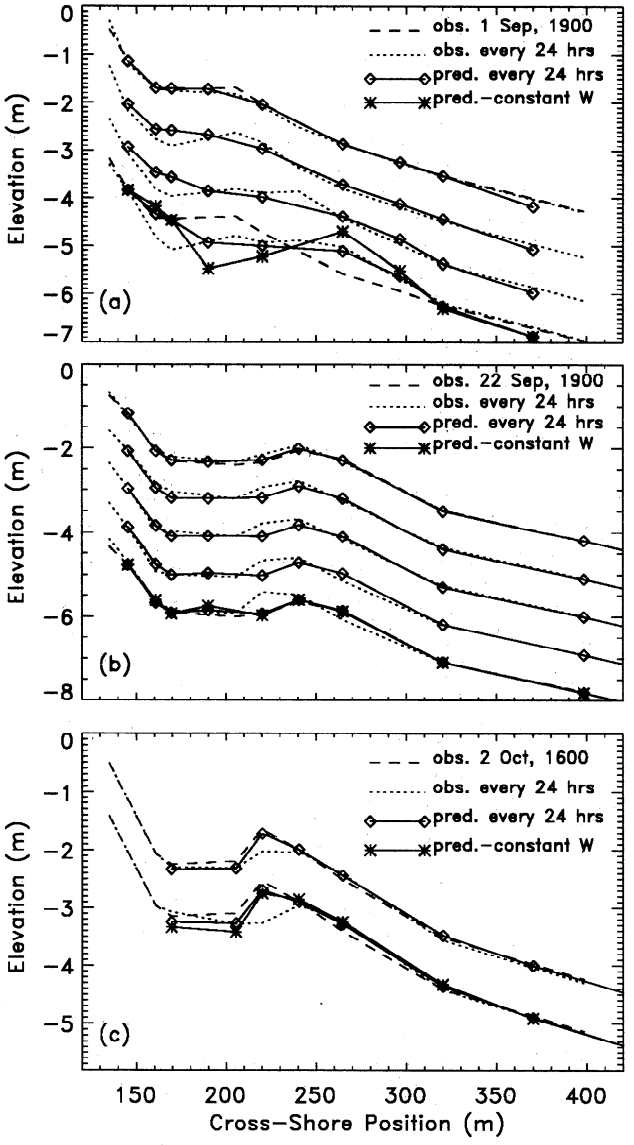

Figure 8. Observed (dotted curves) and predicted (using varying W, solid curves with diamonds) elevation of the seafloor versus cross-shore position. Three-hour average profiles for each 24-hour period after model initialization are sequentially offset by -90 cm in the vertical. The final predicted profiles using constant W (solid curves with asterisks) are also plotted. The initial profiles (dashed curves) are superposed on the final profiles to show total change. (a) Sep 1 1900 – Sep 5 2200, (b) Sep 22 1900 – Sep 27 2200, and (c) Oct 2 1600 – Oct 4 1300.

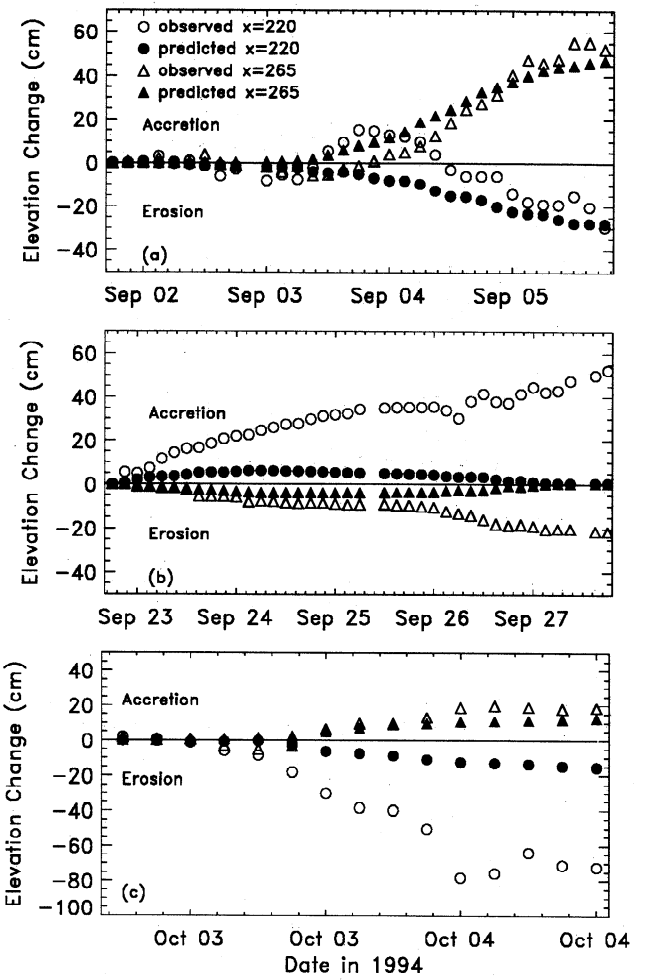

Figure 9. Observed (open symbols) and predicted (solid symbols) seafloor elevation (every 3 hours) at two cross-shore locations (triangles, x=265 m and circles, x=220) for each 3-hour period versus time. (a) Sep 1 1900 – Sep 5 2200, (b) Sep 22 1900 – Sep 27 2200, and (c) Oct 2 1600 – Oct 4 1300.

ures 8c and 9c, skill=0.28, $r = 0.81$ (significant at 95% level)). In this case, high waves ($H_s = 2.5$ m) occurred for a relatively short period and the maximum offshore directed current was relatively low ($\approx$ 30 cm/s, Figure 2). The model has no skill in predicting the approximately 20 m onshore bar movement observed in event b (Figure 8b, skill = 0.02, $r = 0.28$ (not significant)).

The cross-shore bathymetric evolution was predicted over the entire 2-month data set by initializing with the profile observed on September 1 and driving with currents observed every 3-hour period until October 28. As shown in Figure 10a, model skill is high ($\approx$ 0.5) for

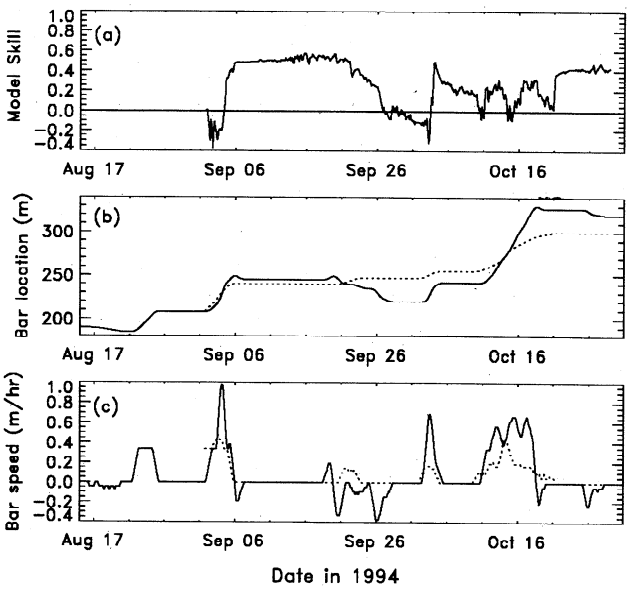

Figure 10. (a) Cumulative model skill, predicted (dotted curve) and observed (solid curve), (b) cross-shore location of the sand bar, and (c) cross-shore migration speed of the sand bar versus time.

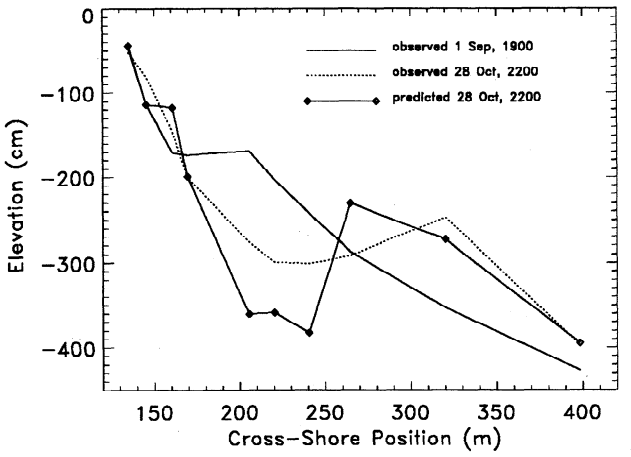

Figure 11. Observed (Sep 1 1900 (initial condition), solid curve, and Oct 28 2200, dotted curve) and predicted (Oct 28 2200, solid curve with diamonds) 3-hour average elevation of the seafloor versus cross-shore position.

the first 20 days and then decreases to ≈ 0 between September 20 and October 2, which includes event b and the period of greatest onshore bar migration (Figure 2b). During the period of low skill, the bar crest is about midway between the initial and the predicted locations (Figure 10b). On October 16, 60 days after initialization, the bar moves offshore, the skill increases to about 0.4, and the predicted and observed profile changes are similar ($r = 0.89$ (significant at the 95% level), Figure 11). The predicted maximum offshore migration rates of the sand bar (Figure 10c) (based on the predicted location of the bar crest, Figure 10b) are about half of the observed rates. Onshore migration was not predicted. Predictions and observations of 3-hour averaged seafloor change at four cross-shore locations for the entire 2-month period are shown in Figure 12. At some locations the model predicts elevation change when it was observed (e.g., Figures 12c and 12d), but errors increase at locations where onshore bar migration is modeled poorly (e.g., September 22 – 27 at $x = 220$ m, Figure 12b).

The terms in the total cross-shore sediment transport Q_x can be examined separately. The first three terms on the right hand side of (3) represent bedload transport and the second three correspond to suspended load. The three terms of each group represent transport driven by asymmetries in the oscillatory flow $\tilde{u}$, by the mean flow $\overline{u}$, and by gravity, respectively. Previous model studies [*Stive*, 1986; *Thornton et al.*, 1996] suggest that the gravity-driven and bedload transport

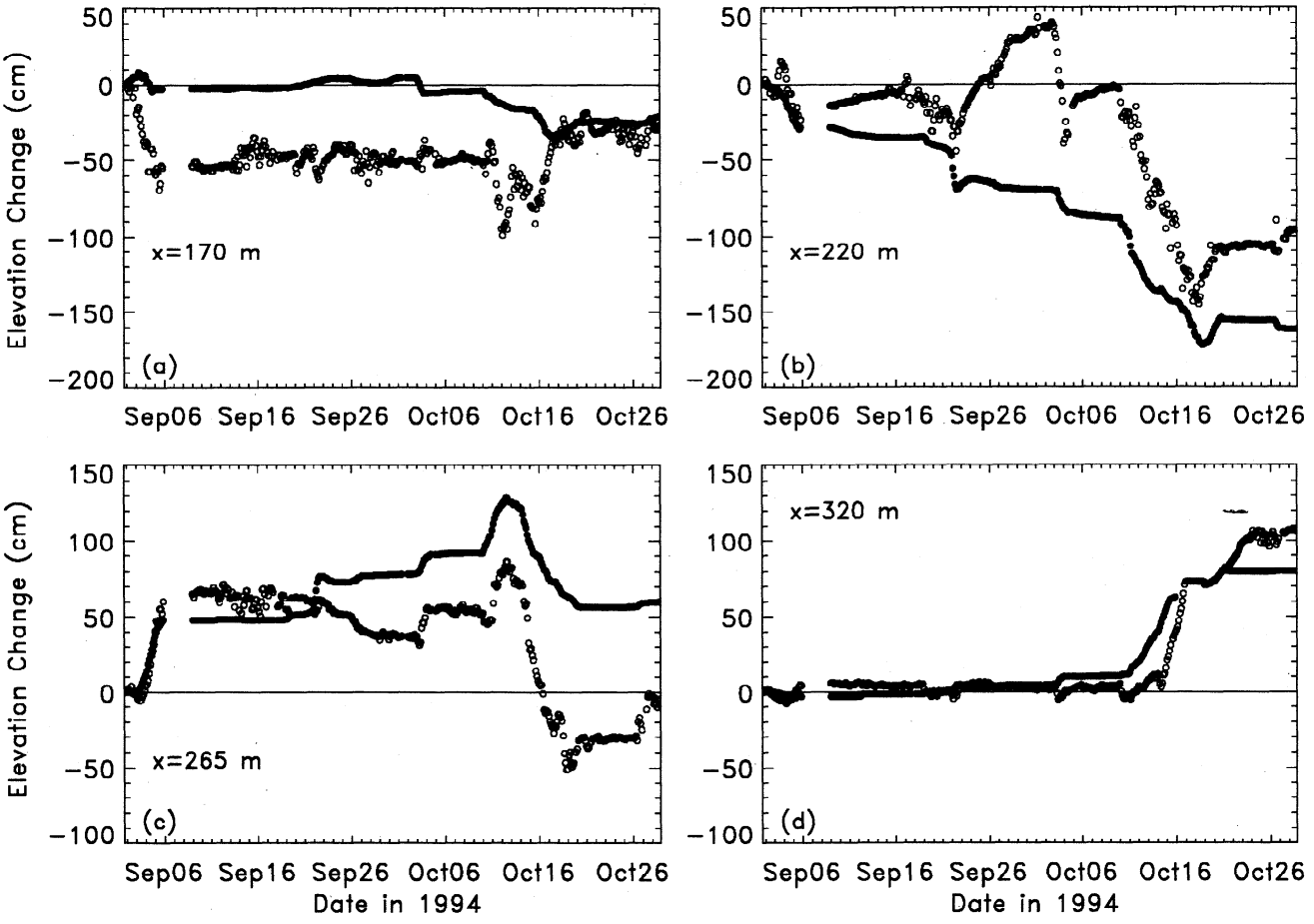

Figure 12. Observed (open circles) and predicted (solid circles) change in seafloor elevation at four cross-shore locations for every 3-hour period between Sep 1 1900 and Oct 28 2200 versus time. (a) $x = 170$, (b) $x = 220$, (c) $x = 265$, and (d) $x = 320$ m.

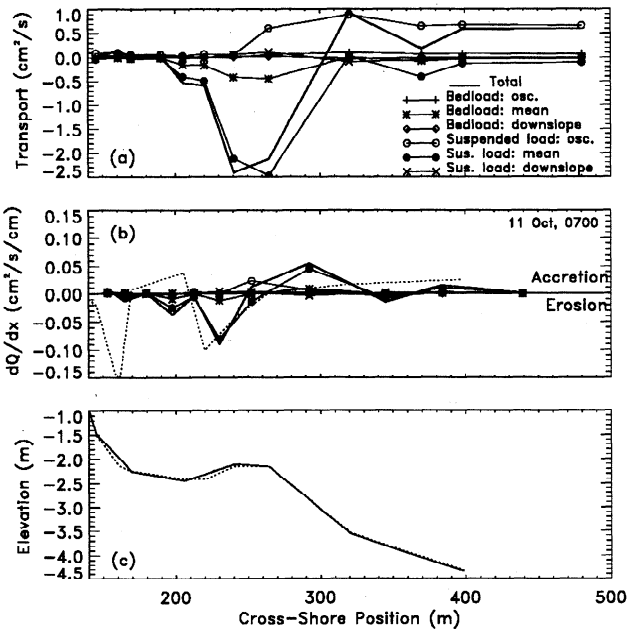

Figure 13. (a) Three-hour average predicted sediment transport for Oct 11 0700–1000 versus cross-shore position. The line types for transport predicted by each of the six terms in the model (equation (3)) are given in the legend and the thick solid curve is the total predicted transport. (b) Cross-shore gradients in each predicted transport term (same line types as Figure 13a) and observed (dotted curve) total transport gradient. (c) Cross-shore profile observed Oct 11 0700 (solid curve) and Oct 11 1000 (dotted curve).

terms are relatively small on a natural beach, as is the case here. Suspended load driven by oscillatory and mean currents dominates the predicted total cross-shore transport Q_x in all cases, as shown for intense storm conditions (October 11, event d) in Figure 13a.

Changes in the profile result from gradients in the cross-shore transport dQ_x/dx (equation (4)) (dQ_y/dy is assumed to be small). During storm event d, dQ_x/dx is dominated by gradients in the mean-flow-driven suspended load transport which result in erosion on the shoreward side of the bar crest and accretion offshore (solid circles in Figure 13b). Other modeled gradient terms are relatively small, except for gradients in the oscillatory-flow-driven suspended transport that results in accretion near the bar crest (open circle at $x = 250$ m in Figure 13b). In storm event a, gradients of mean- and oscillatory-flow-driven suspended transport contribute roughly equally to dQ_x/dx over much of the profile (Figure 14a). The predicted gradients in total cross-shore transport are similar to observed values in these two storms (compare dashed with solid curves in Figures 13b and 14a). Although the modeled total cross-shore transport gradient is underpredicted for storm c (Figure 14c), the trend (erosion in the trough and accretion offshore) is reproduced (compare dashed and solid lines in Figure 14c). In all three storms, measured offshore directed mean flows were maximum just shoreward of the bar crest, and the large gradients in these flows tend to move the bar offshore. The model predicts no significant profile change when wave energy was low and steady flows were weak (event b, Figure 14b). Onshore bar migration was observed in this case.

5. Discussion

The energetics transport model was developed for unidirectional river flows [*Bagnold*, [1966]. The model for combined mean and oscillatory flow (equation (3)) is based on the assumption that sediment suspension occurs instantaneously in response to fluid forcing, so the fluid velocity, sediment suspension, and transport are all in phase. However, sediment suspended at one phase of the wave can be transported during a subsequent phase before settling to the bed [*Hanes and Hunt-*

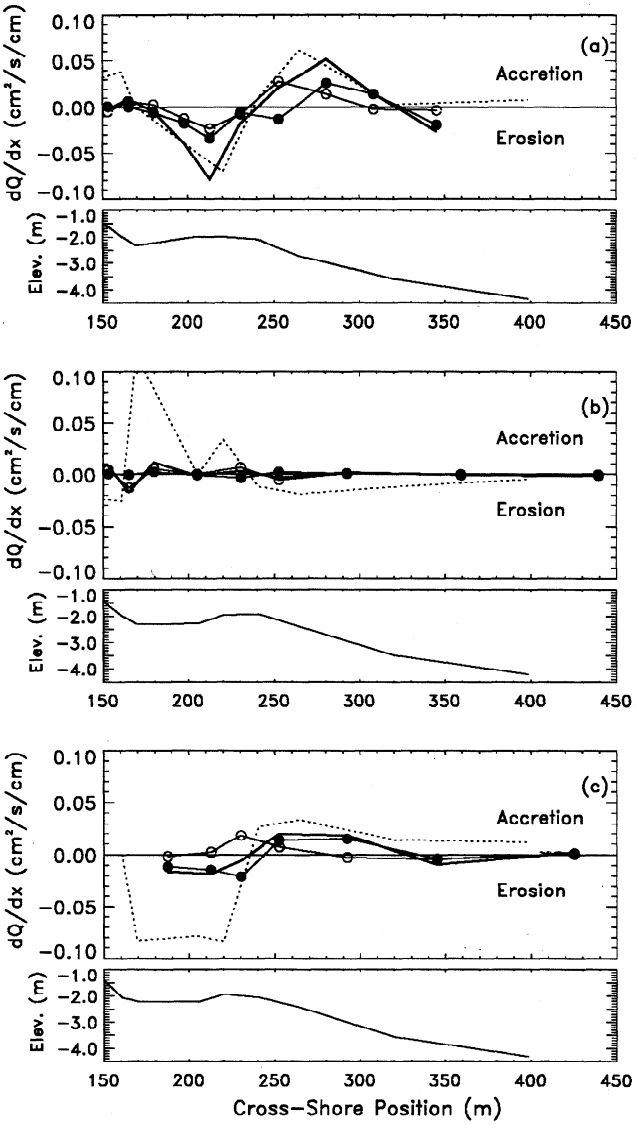

Figure 14. Three-hour average gradients in predicted mean- (solid circles) and oscillatory-flow-driven (open circles) suspended sediment transport, predicted total transport (thick solid curves), and observed transport (dotted curves). The corresponding cross-shore profile is shown in the bottom panels. (a) Sep 4 1000–1300, (b) Sep 26 1000–1300, and (c) Oct 3 1900–2200.

ley, 1986]. Sediment-laden vortices in the wake of ripples or megaripples may alter the amount of suspended sediment relative to that above a flat bed and may also enhance the phase lag between suspension and transport [*Inman and Bowen*, 1963]. Additionally, sediment transport in oscillatory flow may depend on fluid accelerations that are not accounted for in the present model [*Hallermeier*, 1982; *Hanes and Huntley*, 1986]. The energetics model is therefore expected to perform best for flows dominated by quasi-steady currents with sheet flow conditions over a smooth bed [*Roelvink and Stive*, 1989]. *Thornton et al.* [1996] found the best agreement between observed and predicted profile changes when the steady longshore current contributed significantly to mobilizing sediment that was subsequently transported offshore by the mean cross-shore flow.

The 60 days of data were subdivided into five periods with significant profile evolution and five periods of little or no change (dates are given in Table 1 and Figure 15). As discussed above (e.g., Figure 6) megaripples were often present. An RMS bed roughness, indicative of the bedform amplitude, was determined at each altimeter for each 3-hour time period and model skill is not significantly correlated with average (across the transect) RMS bed roughness ($r = 0.27$). Model skill is correlated with the ratio of the maximum (near the bar crest) average (over the modeled period) mean velocity to the maximum average root mean square velocity

$$\frac{\langle(\overline{u}^2 + \overline{v}^2)^{1/2}\rangle}{\langle(\langle\tilde{u}^2\rangle + \langle\tilde{v}^2\rangle)^{1/2}\rangle}$$

(Figure 15, $r = 0.71$, significant at the 95% level). The model skill is highest during the four periods when mean currents are dominant and the profile changes significantly (open symbols with skill > 0.25 in Figure 15). Model skill is low for the six periods when the oscillatory flow is dominant and there is either relatively little profile evolution (solid symbols) or onshore bar migration (open diamond). Perhaps the effects of megaripples increase in importance as oscillatory currents become dominant. Additionally, bed stress and sediment transport may depend on fluid accelerations (not included in the model) when oscillatory flow is dominant.

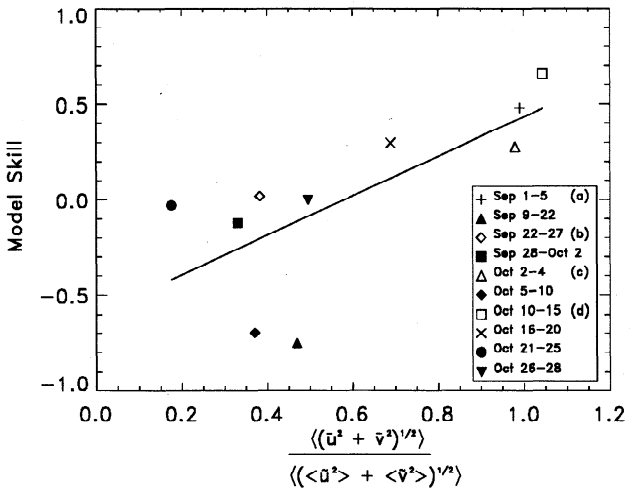

Figure 15. Model skill versus ratio of mean to RMS oscillatory flow. Solid filled symbols are periods of little or no bar migration. Open symbols are periods of largest profile change. The solid line is a least squares fit to all data points ($r = 0.7$, significant at the 95% level).

There are numerous other possible errors in addition to those in the sediment transport model. Vertical shear in the mean cross-shore current may be significant, but the observed mean ($\sim$ 50 cm above the bed) is used directly in the transport equation (equation (3)). Gradients in the alongshore sediment transport are neglected in the profile change model (equation (4)), but the bathymetry after mid-October was irregular in the alongshore direction. The beach change model is based on limited understanding of both sediment and hydrodynamic processes, but does parameterize the dependence of sediment transport gradients (which cause morphology change) on the flow during high-energy conditions.

6. Conclusions

Nearshore morphology and currents were measured nearly continuously for 2 months near Duck, North Carolina. Newly developed sonar altimeters were used to estimate the location of the seafloor along a cross-shore transect, even during storms when traditional surveying techniques fail. The sand bar crest moved approximately 130 m offshore, at rates O(60 cm/h), primarily during three periods with energetic waves (offshore significant wave heights > 2 m). Slight onshore bar migration was observed under small waves.

An energetics-based sediment transport model predicts accurately the seaward bar motion observed when waves are energetic and near-bottom offshore directed mean currents (e.g., undertow) are strong. Model performance is improved by including cross-shore varying fall velocity (obtained from observed grain size). The dynamics of breaking waves on sand bars are understood only qualitatively, but bar-intensified breaking during storms causes a maximum in the undertow just shoreward of the bar crest, and the predicted offshore bar migration is driven by corresponding gradients in the modeled suspended sediment transport. For low-energy conditions, wave breaking on the bar and mean currents are reduced, and the bar migrates slowly shoreward. The observed onshore bar motion is not predicted, possibly because the model does not include the effects of fluid acceleration nor the effects of phase lags between fluid and sediment, both of which may be important when oscillatory wave velocities dominate the flow.

Integrated over long times, onshore and offshore migration balance on a beach that is not loosing or gaining sand. However, periods of low waves in the present experiment were not prolonged, and profile changes were dominated by well-modeled offshore bar movement. Thus even though the energetics sediment trans-

port model was developed for steady flow over smooth riverbeds and may be inaccurate for wave-dominated flows over ripples and megaripples, the model predicts qualitatively the offshore bar migration and cross-shore profile evolution observed during this stormy 2-month period.

Appendix: Model Sensitivity

Model skill was calculated for the offshore bar migration observed October 10 – 15 (event d) for $0.005 \leq \epsilon_s \leq 0.04$ (with fixed ϵ_b and C_f) and $0.002 \leq \epsilon_b \leq 0.50$ (with fixed ϵ_s and C_f). The highest skills are for $\epsilon_s = 0.015$ and $\epsilon_b = 0.135$ (Table A1). The sensitivity to ϵ_s is much greater than to ϵ_b, consistent with the dominance of suspended load compared with bed load transport (Figure 13). The skill is not sensitive to variation of ϵ_s over the range 0.01 – 0.02.

Church and Thornton [1993] suggest $0.001 \leq C_f \leq 0.006$. Although model skill (with fixed ϵ_s and ϵ_b) is not effected greatly for $0.002 \leq C_f \leq 0.004$, C_f values outside this range result in significantly decreased skill (Table A1).

The model predictions also are not sensitive to plausible measurement errors. For each of 100 simulations of event d, a random offset uniformly distributed between ±6 cm/s was applied to each current meter for the duration of the event (representing a quasi-stable offset error with magnitude roughly representative of the errors in these observations). The simulations produced a mean model skill of 0.5 with a relatively small standard deviation of 0.1. Likely errors in the orientations of the current meters (±5°) resulted in a mean model skill of 0.65, with standard deviation of 0.02. The model skill for event d also varied by less than 10% when a few arbitrarily selected sensors were excluded from the model-data comparisons.

Table A1. Model Skills: October 10 – 15, Event d

	$\epsilon_s = 0.015$ $\epsilon_b = 0.135$	$C_f = 0.003$ $\epsilon_b = 0.135$	$C_f = 0.003$ $\epsilon_s = 0.015$
$\epsilon_s = 0.005$		0.41	
$\epsilon_s = 0.01$		0.60	
$\epsilon_s = 0.015$		0.66	
$\epsilon_s = 0.02$		0.53	
$\epsilon_s = 0.04$		-0.35	
$\epsilon_b = 0.002$			0.65
$\epsilon_b = 0.135$			0.66
$\epsilon_b = 0.5$			0.37
$C_f = 0.001$	0.31		
$C_f = 0.002$	0.57		
$C_f = 0.003$	0.66		
$C_f = 0.004$	0.48		
$C_f = 0.006$	-0.12		

Model skill (section 4) using a range of values for ϵ_s and ϵ_b from *Bailard* [1982] and a range of values for C_f from *Church and Thornton* [1993].

Acknowledgments. This research was funded by the Office of Naval Research (Coastal Dynamics and AASERT graduate student support) and the National Science Foundation (Coastal Ocean Processes program). The instruments were fabricated, deployed, and maintained by staff from the Center for Coastal Studies. The U.S. Army Corps of Engineers Field Research Facility provided excellent logistical support. T.H.C. Herbers and B. Raubenheimer helped collect the field data. Brad Werner and E.B. Thornton made many valuable comments and E.B. Thornton generously provided information from previous studies.

References

Aubrey, D.G., Seasonal patterns of onshore/offshore sediment movement, *J. Geophys. Res., 84*, 6347–6354, 1979.

Bagnold, R.A., An approach to the sediment transport problem from general physics, *Prof. Paper 422-I* U.S. Geol. Surv., 1966.

Bailard, J.A., An energetics total load sediment transport model for a plane sloping beach, *J. Geophys. Res., 86*, 10938–10954, 1981.

Bailard, J.A., Modeling on-offshore sediment transport in the surf zone, in *Proc. 18th Int. Coastal Eng. Conf.* pp 1419–1438, Am. Soc. of Civ. Eng., New York, 1982.

Bailard, J.A., and D.L. Inman, An energetics bedload transport model for a plane sloping beach: local transport, *J. Geophys. Res., 86*, 2035–2043, 1981.

Bowen, A.J., Simple models of nearshore sedimentation; beach profiles and longshore bars, in *The Coastline of Canada*, edited by S.B. McCann, Geol. Surv. of Can. *Pap. 80-10*, pp 1–11, Ottawa, 1980.

Bruun, P., Coast erosion and the development of beach profiles, *Tech. Memo. 44*, U.S. Army Corps of Eng., Beach Erosion Board, 1954.

Church, J.C., and E.B. Thornton, Effects of breaking wave induced turbulence within a longshore current model, *Coastal Eng., 20*, 1–28, 1993.

Conley, D.C., and D.L. Inman, Field observations of the fluid-granular boundary layer under nearbreaking waves *J. Geophys. Res., 97*, 9631–9643, 1992.

Conley, D.C., and D.L. Inman, Ventilated oscillatory boundary layers, *J. Fluid Mech., 273*, 261–284, 1994.

Dally, W.R., and R.G. Dean, Suspended sediment transport and beach profile evolution, *J. Waterw. Port Coastal Ocean Eng., 110*, 15–33, 1984.

Davis, R.E., Predictability of sea surface temperature and sea level pressure anomalies over the North Pacific Ocean, *J. Phys. Oceanogr., 6*, 249–266, 1976.

Dean, R.G., Equilibrium beach profiles: U.S. Atlantic and Gulf coasts, *Ocean Eng. Rep. 12*, Dep. of Civil Eng., Univ. of Delaware, 1977.

Dyhr-Nielsen, M., and T. Sorensen, Sand transport phenomena on coasts with bars, in *Proc. 12th Int. Coastal Eng. Conf.*, pp 855–866, Am. Soc. of Civ. Eng., New York, 1970.

Downing, J.P., R.W. Sternberg, and C.R.B. Lister, New instrumentation for the investigation of sediment suspension processes in the shallow marine environment, *Mar. Geol., 42*, 19–34, 1981.

Eagleson, P.S., and R.G. Dean, Wave-induced motion of bottom sediment particles, *ASCE Trans., 126*, 1162–1189, 1961.

Foster, D.L., R.A. Holman, and R.A. Beach, Sediment suspension events and shear instabilities in the bottom boundary layer, in *Coastal Dynamics '95*, pp 712–726, Am. Soc. of Civ. Eng., New York, 1995.

Gallagher, E.L., W. Boyd, S. Elgar, R.T. Guza, and B. Woodward, Performance of a sonar altimeter in the nearshore, *Mar. Geol., 133*, 241–248, 1996.

Haines, J.W., and A.H. Sallenger, Vertical structure of mean cross-shore currents across a barred surf zone, *J. Geophys. Res., 99*, 14223–14242, 1994.

Hallermeier, R., Oscillatory bedload transport: data review and simple formulation, *Cont. Shelf Res., 1*, 159–190, 1982.

Hanes, D.M., and D.A. Huntley, Continuous measurements of suspended sand concentration in a wave dominated nearshore environment, *Cont. Shelf Res., 6*, 585–596, 1986.

Hay, A.E., and A.J. Bowen, Coherence scales of wave-induced suspended sand concentration fluctuations, *J. Geophys. Res., 99*, 12,749–12,765, 1994.

Hay, A.E., and A.J. Bowen, Space-time variability of sediment suspension in the nearshore zone, *Coastal Dynamics '95*, pp 962–975, Am. Soc. of Civ. Eng., New York, 1995.

Hay, A.E., and D.J. Wilson, Rotary sidescan images of nearshore bedform evolution during a storm, *Mar. Geol., 119*, 57–65, 1994.

Holman, R.A., and A.J. Bowen, Bars, bumps and holes: models for the generation of complex beach topography, *J. Geophys. Res., 87*, 457–468, 1982.

Holman, R.A., and A.H. Sallenger, Sand bar generation: A discussion of the Duck experiment series, *J. Coastal Res., 15*, 76–92, 1993.

Inman, D.L., and A.J. Bowen, Flume experiments on sand transport by waves and currents, in *Proc. 8th Int. Coastal Eng. Conf.*, pp 137–150, Am. Soc. of Civ. Eng., New York, 1963.

Jaffe, B.E., R.W. Sternberg, and A.H. Sallenger, The role of suspended sediment in shore-normal beach profile changes, in *Proc. 19th Int. Coastal Eng. Conf.*, pp 1983–1996, Am. Soc. of Civ. Eng., New York, 1984.

Kraus, N.G., and M. Larson, Prediction of initial profile adjustment of nourished beaches to wave action, in *Proc. Beach Technology '88*, pp 125–137, Fl. Shore and Beach Preserv. Assoc., Jacksonville, Fla., 1988.

Kriebel, D.L., and R.G. Dean, Numerical simulations of time-dependent beach and dune erosion, *Coastal Eng., 9*, 221–245, 1985.

Lee, G., and W. A. Birkemeier, Beach and nearshore survey data: 1985–1991, CERC Field Research Facility, *Tech. Rep. CERC-93-3*, U.S. Army Corps of Eng., Waterways Exp. Stn., Vicksburg, Miss., 1993.

Lippmann, T.C. and R.A. Holman, The spatial and temporal variability of sand bar morphology, *J. Geophys. Res., 95*, 11575–11590, 1990.

Lippmann, T.C., E.B. Thornton, and A.J.H.M. Reniers, Wave stress and longshore current on barred profiles, in *Coastal Dynamics '95*, pp 401–412, Am. Soc. of Civ. Eng., New York, 1996.

Masselink, G. and K.P. Black, Magnitude and cross-shore distribution of return flow measured on natural beaches, *Coastal Eng., 25*, 165–190, 1995.

Nairn, R.B. and H.N. Southgate, Deterministic profile modeling of nearshore processes. Part 2. Sediment transport and beach profile development, *Coastal Eng., 19*, 57–96, 1993.

Roelvink, J.A. and I. Brøker, Cross-shore profile models, *Coastal Eng., 21*, 163–191, 1993.

Roelvink, J.A., and M.J.F. Stive, Bar generating cross shore flow mechanisms on a beach, *J. Geophys. Res., 94*, 4785–4800, 1989.

Sallenger, A.H. and P.A. Howd, Nearshore bars and the break-point hypothesis, *Coastal Eng., 12*, 301–313, 1989.

Sato, S. and N. Mitsunobu, A numerical model of beach profile change due to random waves, in *Proc. Coastal Sediments '91*, pp 674–687, Am. Soc. Civil Eng., New York, 1991.

Seymour, R.J., Nearshore auto-suspending turbidity flows, *Ocean Eng., 13*, 435–447, 1986.

Seymour, R.J., An assessment of NSTS, in *Proc. Coastal Sediments '87*, 642–651, Am. Soc. Civil Eng., New York, 1987.

Sleath, J.F.A., *Sea Bed Mechanics*, 335 pp, John Wiley, New York, 1984.

Smith, J.M., I.A. Svendsen, and U. Petrevu, Vertical structure of the nearshore current at DELILAH: measured and modeled, in *Proc. 23rd Int. Coastal Eng. Conf.*, pp 2825–2838, Am. Soc. Civil Eng., New York, 1992.

Stauble, D.K., Long-term profile and sediment morphodynamics: Field Research Facility case history, *Tech. Rep. CERC-92-7*, U.S. Army Corps of Eng., 1992.

Stive, M.J.F., A model for cross-shore sediment transport, in *Proc. 20th Int. Coastal Eng. Conf.*, pp 1550–1564, Am. Soc. Civil Eng., New York, 1986.

Stive, M.J.F. and J.A. Battjes, 1984: A Model for Offshore Sediment Transport, in *Proc. 19th Int. Coastal Eng. Conf.*, pp 1420–1436, Am. Soc. Civil Eng., New York, 1984.

Stive, M.J.F. and H.G. Wind, Cross-shore mean flow in the surf zone, *Coastal Eng., 6*, 1–25, 1986.

Svendsen, I.A. and J. Buhr Hansen, Cross-shore currents in surf-zone modelling, *Coastal Eng., 12*, 23–42, 1988.

Takeda, I., and T. Sunamura, Beach changes by storm waves, in *Proc. 20th Int. Coastal Eng. Conf.*, pp 1612–1622, Am. Soc. Civil Eng., New York, 1986.

Thornton, E.B., R.T. Humiston, and W. Birkemeier, Bar–trough generation on a natural beach, *J. Geophys. Res., 101*, 12097–12110, 1996.

Watanabe, A. and M. Dibajnia, Numerical modeling of nearshore waves, cross shore sediment transport and beach profile change, in *Proc. Int. Assoc. for Hydraul. Res., Symposium on Mathematical Modeling of Sediment Transport in the Coastal Zone*, Copenhagen, pp 166-174, 1988.

Winant, C.D., D.L. Inman, and C.E. Nordstrom, Description of seasonal beach changes using empirical eigenfunctions, *J. Geophys. Res., 80*, 1979–1986, 1975.

Wright, L.D. and A.D. Short, Morphodynamic variability of surf zones and beaches: a synthesis, *Mar. Geol., 26*, 93–118, 1984.

S. Elgar, School of Electrical Engineering and Computer Science, Washington State University, Pullman, WA 99164-2752. (email: elgar@eecs.wsu.edu)

E.L. Gallagher, Oceanography Department, Naval Postgraduate School, 833 Dyer Rd., Rm. 328, Monterey, CA 93943-5122. (email: egallagh@oc.nps.navy.mil)

R.T. Guza, Center for Coastal Studies, Scripps Institution of Oceanography, University of California San Diego, 9500 Gilman Dr., La Jolla, CA 92093-0209. (email: rtg@coast.ucsd.edu)

(Received January 15, 1997; revised June 21, 1997; accepted August 15, 1997.)